REVIEW

Check for updates

Journal of
Sensor Science and Technology

The Korean Sensors Society

Recent Advances and Challenges of Two-Dimensional MXene-based Chemoresistive Gas Sensors

Gi Baek Nam[1] and Ho Won Jang[1,2,+]

[1]*Department of Materials Science and Engineering, Research Institute of Advanced Materials, Seoul National University, Seoul 08826, Republic of Korea*
[2]*Advanced Institute of Convergence Technology, Seoul National University, Suwon 16229, Republic of Korea*

Cite This: *J. Sens. Sci. Technol. Vol. 34, No. 4 (2025) 375-386*

https://doi.org/10.46670/JSST.2025.34.4.375

ABSTRACT: The rise of the Internet of Things (IoT) and artificial intelligence has made chemical sensors crucial for applications such as environmental monitoring, hazardous chemical detection in industry, smart farming, and medical diagnostics. Among various sensor types, chemoresistive gas sensors are particularly well-suited for IoT integration due to their simple design, low manufacturing cost, and strong compatibility with electronic systems. However, conventional metal oxide-based sensors face limitations, requiring high operating temperatures and having rigid atomic structures, which restrict their use in emerging technologies like wearable and biocompatible sensors. MXene, a class of two-dimensional transition metal carbides, nitrides, and carbonitrides, has gained attention for its potential in sensing applications. This is due to its high electrical conductivity, ease of surface modification, mechanical flexibility, and large surface area. In this review, we provide an overview of recent advancements in MXene synthesis and its role in chemoresistive gas sensing. We also discuss the underlying mechanisms that allow MXene to detect gases at room temperature. Furthermore, we examine strategies such as surface functionalization and the formation of heterostructures with nanocomposites to improve the sensitivity and selectivity of MXene-based sensors for specific analytes, including NO_2, NH_3, and C_2H_5OH. Finally, we highlight current challenges and suggest promising avenues for future research to develop practical, multifunctional MXene-based gas sensors.

KEYWORDS: *MXene, Two-dimensional materials, Chemoresistive gas sensor, Chemical sensor, $Ti_3C_2T_x$, Flexible sensor*

1. INTRODUCTION

With the rapid advancement in artificial intelligence (AI), the demand for sensors capable of detecting pressure, gas, liquid, and light has increased owing to their integration with Internet of Things (IoT) technologies [1,2]. Gas sensors are crucial for applications such as human health diagnostics, environmental monitoring, smart agriculture, and industrial safety [3-5]. Among gas sensors, chemoresistive sensors detect gas molecules by measuring changes in electrical resistance. This offers advantages such as a simple device structure, low fabrication cost, and easy integration with electronic components, making them ideal for IoT systems [6,7]. Metal oxide-based materials have dominated chemoresistive gas sensors due to their high sensitivity, chemical stability, and reliable performance [8,9]. However, metal oxide sensors typically require operating temperatures between 200°C and 400°C due to their high activation energies [10]. High-temperature operation introduces challenges such as increased fabrication complexity, high power consumption, and difficulties in deploying sensors in wearable or portable devices. To enable gas detection at room temperature, 2-dimensional (2D) materials, such as graphene [11,12], halide perovskite (HP) [13], and transition metal dichalcogenides (TMDs) [14-16], have been used owing to their high surface-to-volume ratio and relatively low activation energies. However, graphene-, HP-, and TMD-based gas sensors generally exhibit slow responses, low recovery rates, and poor selectivities.

Recently, MXenes, a family of 2D hexagonal carbides, nitrides, and carbonitrides, have emerged as promising materials for room-temperature gas sensing (Fig. 1) [17,18]. MXene materials have the general formula $M_{n+1}X_nT_x$, where M represents an early transition metal (such as Co, Cr, Ti, or Zr), X is carbon or nitrogen, and T_x denotes surface termi-

+Corresponding author: hwjang@snu.ac.kr
Received : Jun. 20, 2025, Revised : Jun. 29, 2025, Accepted : Jul. 11, 2025

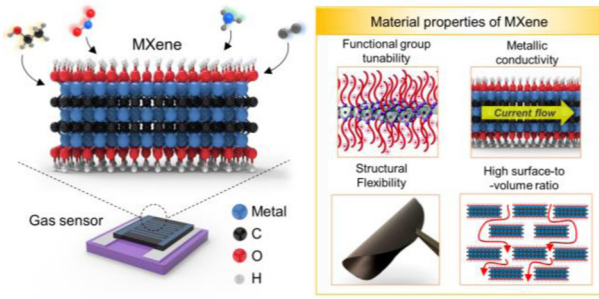

Fig. 1. Schematic illustration of MXene-based gas sensors, highlighting the structural, electronic, and surface chemical properties relevant to gas sensing. Reprinted with permission from Ref. [29], Copyright (2019) American Chemical Society. Reprinted with permission from Ref. [30], Copyright (2015) Royal Society of Chemistry.

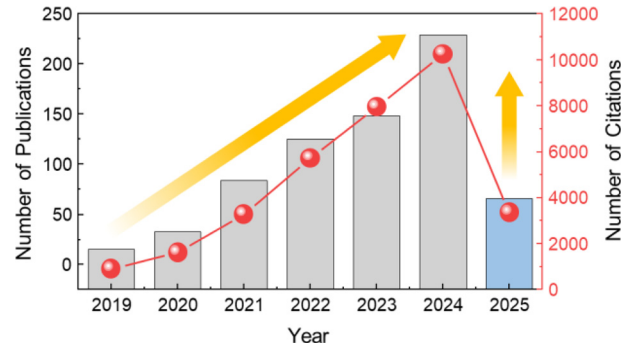

Fig. 2. Number of publications and citations related to MXene-based gas sensors, with data obtained from the Web of Science Core Collection using the keywords "MXene gas sensor" and "MXene gas detection".

nation groups like hydroxyl (-OH), oxygen (-O), and fluorine (-F). MXenes are synthesized by selectively etching an atomic layer (IIIA or IVA elements with Al, Si, Ga, Ge, In, or Sn) from the MAX phases using fluoride-containing acidic solutions, resulting in abundant functional groups on their surfaces. MXene exhibits metallic-level electrical conductivity, provides high electron mobility, and enables the rapid detection of low-concentration gases with reduced signal-to-noise ratios [19]. Additionally, the abundance of surface functional groups facilitates efficient interactions with polar gases, enhancing gas reactivity [20]. Many MXene based gas sensors using $Ti_3C_2T_x$ [21], $V_4C_3T_x$ [22], and Mo_2CT_x [23] been reported for the detection of NO_2, NH_3, CO_2 and volatile organic compounds (VOCs). Moreover, various strategies, such as surface functionalization (ADOPA [24] and FOTS [25]) and heterostructure formation (CuO/Mxene [26], SnO_2/Mxene [27], and WSe_2/Mxene [28]), have been investigated to enhance the gas detection properties. Fig. 2 shows the recent publication trends and citation counts related to MXene-based gas sensors, highlighting the rapidly growing research interest in MXene-based sensor technology.

This review systematically evaluates recent advances in MXene-based gas sensors, focusing on synthesis methods, intrinsic material properties, sensing mechanisms, and potential practical applications. It highlights the unique characteristics of MXenes that enhance the performance of chemoresistive gas sensors, such as tunable surface functional groups, metallic conductivity, structural flexibility, and high surface-to-volume ratios. The review also addresses critical challenges facing MXene gas sensors, including long-term stability, humidity resistance, and integration with AI technologies. Finally, it identifies key future research directions needed to advance MXene-based chemoresistive gas sensors for practical deployment in emerging sensing technologies.

2. FUNDAMENTALS OF MXene-BASED GAS SENSORS

MXene materials have attracted interest for gas-sensing applications owing to their unique properties, including metallic conductivity, versatile surface functionalization, and mechanical flexibility. These characteristics enable MXene-based chemoresistive gas sensors to deliver rapid response and a low signal-to-noise ratio at room temperature, distinguishing MXene from conventional metal oxides and other 2D materials, including TMD and graphene. This section provides a comprehensive overview of the fundamental properties of MXene, its synthesis from MAX phases, its unique structural features, and the gas detection mechanisms of MXene-based gas sensors.

2.1 Synthesis Methods of MXene

MXenes are synthesized by the selective etching of the A atomic layer (elements such as Al, Si, Ga, Ge, In, and Sn) from the MAX phase [31]. MAX phases have distinct bond strengths in M-X and M-A bonding, allowing for the selective removal of the A layers through chemical etching. Gogotsi et al. first demonstrated the synthesis of $Ti_3C_2T_x$ MXenes by selectively removing the Al layer from Ti_3AlC_2 using HF (Fig. 3 (a)). During etching, the Al atoms in Ti_3AlC_2 reacted preferentially with HF to form soluble aluminum fluoride (AlF_3), facilitating the removal of the Al layer. Subsequently, the synthesized MXene was washed and purified using a centrifuge to remove the residual etchant and impurities. Subsequently, MXene was subjected to ultrasonication to facilitate exfoliation. Figs. 3 (b) and 3 (c) present scanning electron microscopy (SEM) images of the $TiAlC_2$ and resulting $Ti_3C_2T_x$, exhibiting a characteristic accordion-like morphology [32]. Similar HF-based etching methods have been used to successfully syn-

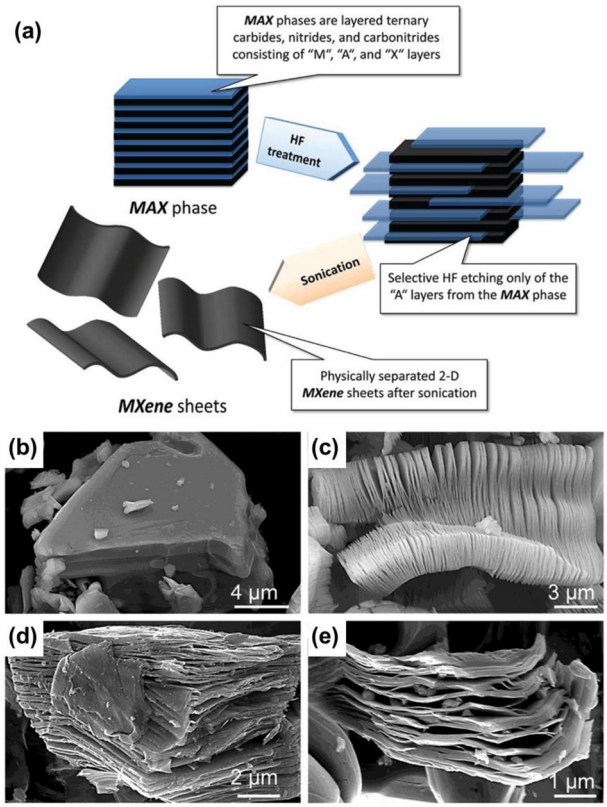

Fig. 3. Synthesis process of MXenes from MAX phases. (a) Schematic illustration of the etching process from MAX phases to MXene. (b) Ti_3AlC_2 particle before treatment, representing unreacted MAX phases, (c) Ti_3AlC_2 after HF treatment, (d) Ti_2AlC after HF treatment, (e) Ta_4AlC_3 after HF treatment. Reprinted with permission from Ref. [31], Copyright (2019) American Chemical Society.

thesize MXenes from other Al-containing MAX phases, such as Ti_2AlC and Ta_4AlC_3, as shown in Figs. 3 (d) and (e).

However, HF etching methods require careful handling owing to the due to the toxicity and surface stabilization issues associated with residual HF. As a result, alternative, milder approaches have been explored, combining HF with less aggressive acids, such as hydrochloric acid (HCl) [33] or sulfuric acid (H_2SO_4) [34]. In particular, lithium fluoride (LiF)- and HCl-based minimally intensive layer delamination (MILD) etching has been developed as an effective method for MXene production [33]. This MILD approach enables high-yield synthesis of defect-free flakes with minimal structural damage. During MILD etching, Li+ ions serve as intercalants, expanding the interlayer spacing and facilitating subsequent delamination. Ghidiu et al. demonstrated MXene synthesis using LiF/HCl mixtures, resulting in hydrophilic MXene with fewer structural defects and larger lateral dimensions compared to the HF-only method [35].

In addition to LiF/HCl-based etching, organic intercalants such as dimethyl sulfoxide (DMSO) [36] and tetramethylammonium hydroxide (TMAOH) [37] have also been employed. Mashtalir et al. reported successful intercalation and delamination of $Ti_3C_2T_x$ MXene using DMSO, resulting in hygroscopic and readily dispersible MXene powders [38]. Similarly, Xuan et al. utilized TMAOH for $Ti_3C_2T_x$ MXene synthesis, demonstrating efficient Al-layer etching by formation of soluble $Al(OH)_4^-$ ions [39]. Moreover, the bulky TMA^+ cations were effectively intercalated between the MXene layers, enhancing the delamination efficiency. Therefore, MXenes are typically synthesized via selective chemical etching from MAX phases using acidic solutions coupled with various intercalation and delamination techniques to produce MXene materials.

2.2 Unique Structural Properties and Sensing Mechanisms of MXene-based Chemoresistive Gas Sensors

MXenes possess several unique properties that make them ideal materials for gas sensors. They feature abundant surface functional groups, such as -F, -OH, and -O, which play a critical role in gas sensing by selectively interacting with target gas molecules. For example, NO_2 shows a strong affinity for -O groups, while acidic gases exhibit enhanced selectivity through hydrogen bonding interactions with -OH groups [20,21]. In terms of mechanical properties, the layered structure of MXenes provides high tolerance under external strain, with the $Ti_3C_2T_x$ monolayer demonstrating a tensile strength of up to 15.4 GPa and a Young's modulus of approximately 0.484 TPa [40]. This combination of mechanical strength and flexibility makes MXenes suitable for flexible gas sensor applications. Additionally, MXenes exhibit metallic-level electrical conductivity, attributed to strong metal-carbon bonding and filled conduction-band states resulting from d-band electrons [41]. Their high conductivity leads to a low signal-to-noise ratio, allowing for effective gas detection at low concentrations. Furthermore, the rapid electron-hole mobilities in MXenes contribute to fast gas-sensing responses and quick recovery times.

The sensing mechanism of MXene gas sensors involves two primary phenomena: charge-transfer interactions between MXenes and gas molecules, and intercalation-induced interlayer swelling. Most MXenes, including $Ti_3C_2T_x$ and $V_4C_3T_x$, exhibit p-type semiconducting properties. In the charge-transfer mechanism, when reducing gases (such as H_2, NH_3, and VOCs) are introduced to MXenes, they donate electrons to the MXene, reducing the hole concentration and increasing electrical resistance [42]. Conversely, when oxidizing gases (such as NO_2 and O_3) are introduced, they accept electrons from the

MXenes, increasing the hole concentration and decreasing the resistance.

Another key mechanism is gas-induced interlayer swelling. The MXene films exhibited an accordion-like layered morphology, with gas molecules entering the interlayer spaces either physically or chemically, causing structural swelling and an increase in interlayer spacing [43]. This expansion disrupts the electron conduction pathways between adjacent MXene layers, leading to an overall increase in electrical resistance. Additionally, the adsorbed gas molecules contribute to electron scattering, which reduces carrier mobility. When the swelling-induced modulation of resistance exceeds the charge transfer effects, the MXene-based sensors show an increase in resistance, regardless of whether the gas is reducing or oxidizing.

3. RECENT PROGRESS IN MXene-based GAS SENSORS

MXenes provide notable advantages for gas sensors owing to their tunable surface functional groups, high conductivity, and high surface-to-volume ratios. Surface functional groups facilitate strong interactions with gas molecules, and high electrical conductivity reduces noise and improves detection limits. Various MXene-based gas sensors including $Ti_3C_2T_x$ [44], Nb_2CT_x [45], V_2CT_x [46], and $Mo_2TiC_2T_x$ [47] have been extensively investigated for the detection of diverse gases, including NO_2, NH_3, ethanol, acetone, and humidity. However, pristine MXenes exhibit limitations, including low response signals and humidity instability, which hinder their practical sensor applications. To address these challenges, the enhancement of MXene sensing performance has been explored through controlled surface functionalization and the creation of heterojunctions with nanostructures. Surface functionalization, such as polymer or fluorine treatment, improves MXenes' reactivity to specific gases, as well as their long-term and humidity stability [25]. In the case of heterojunctions, MXenes form composites with TMDs or metal oxides, leading to a high response to target gases through numerous junctions [28]. This section comprehensively discusses recent advances in pristine MXene-based gas sensors, surface functionalization of MXenes, and MXene-based nanocomposite heterostructures, highlighting specific strategies and performance improvements.

3.1 Gas Sensors Based on Pristine MXenes

Various pristine MXenes, including $Ti_3C_2T_x$, Nb_2CT_x, V_2CT_x, and $Mo_2TiC_2T_x$ have been explored as chemoresistive gas sensors. Kim et al. reported a pristine $T_3C_2T_x$ MXene gas sensor for the detection of VOCs at low concentrations (50-100 ppb), which was synthesized by selective Al-layer etching from Ti_3AlC_2 using a LiF/HCl etchant (Fig. 4 (a)) [21]. The sensors were fabricated by coating $Ti_3C_2T_x$ flakes between gold electrodes. The sensor response, defined as resistance variation relative to baseline resistance ($\Delta R/R_b$ (%)), was tested with gases including acetone, ethanol, ammonia, propanal, NO_2, SO_2, and CO_2 (Fig. 4 (b)). The highest sensor response was observed for ethanol (1.7%), as shown in Fig. 4 (c). In particular, acidic gases showed high responses, which were attributed to strong interactions with the-OH groups on the $Ti_3C_2T_x$ surfaces. Fig. 4 (d) compares $Ti_3C_2T_x$ responses with other 2D materials, including reduced graphene oxide (RGO), MoS_2, and black phosphorus (BP), for the detection of 100 ppm acetone, ethanol, and ammonia. Semiconducting materials with BP and MoS_2 demonstrated higher responses to ammonia, whereas those with RGO and $Ti_3C_2T_x$ exhibited stronger responses to VOCs. $Ti_3C_2T_x$ exhibited a positive response to both ammonia (reducing) and NO_2 (oxidizing), enabling effective discrimination between the gases (Fig. 4 (e)). $Ti_3C_2T_x$ exhibited the lowest measured signal-to-noise ratio (0.005%) under N_2 flow, outperforming BP (1.5%), MoS_2 (1.0%), and RGO (0.02%), owing to its high electrical conductivity of $Ti_3C_2T_x$. Thus, the pristine Ti3C2Tx MXene demonstrated superior sensing performance for VOC detection at room temperature with excellent low-concentration sensitivity.

In addition to $Ti_3C_2T_x$, other MXenes such as Nb_2CT_x and V_2CT_x, have also been widely investigated as target gases. Lee et al. demonstrated a V_2CT_x MXene-based gas sensor for the room-temperature detection of H_2 at the ppm level (Fig. 4 (g)) [48]. V_2CT_x was synthesized from the V_2AlC MAX phase via HF etching for selective Al removal. After etching, tetra-n-butyl ammonium ions (TBA^+) were used for intercalation to delaminate the V_2CT_x sheets (d-V_2CT_x) with ~1.75 thickness. The surface of d-V_2CT_x exhibited highly active states owing to the presence of–F,–O, and–OH functional groups. X-ray photoelectron spectroscopy (XPS) analysis confirmed the presence of surface species such as V-O, V-C-O, V-C-$(OH)_x$, and fluorine terminations (V-F and C–F bonds). Gas-sensing performance tests of the d-V_2CT_x films showed an increase in resistance upon exposure to reducing gases, indicating p-type sensing behavior. The responses ($\Delta R/R_b$) at 100 ppm gas exposure were 0.2435 (H_2), 0.0816 (ethanol), 0.0226 (acetone), 0.0166 (ammonia), 0.0167 (methane), and 0.005 (H_2S). The highest response to H_2 gas was attributed to the active vanadium surface sites, similar to those of vanadium oxide and V-doped metal oxides [49,50]. The response and recovery times to H2 (reaching 90% of the steady-state response) were 2 and 7 min, respectively, with a theoretical detection limit of 1.375 ppm, calculated using a signal-to-noise ratio of 3. These results

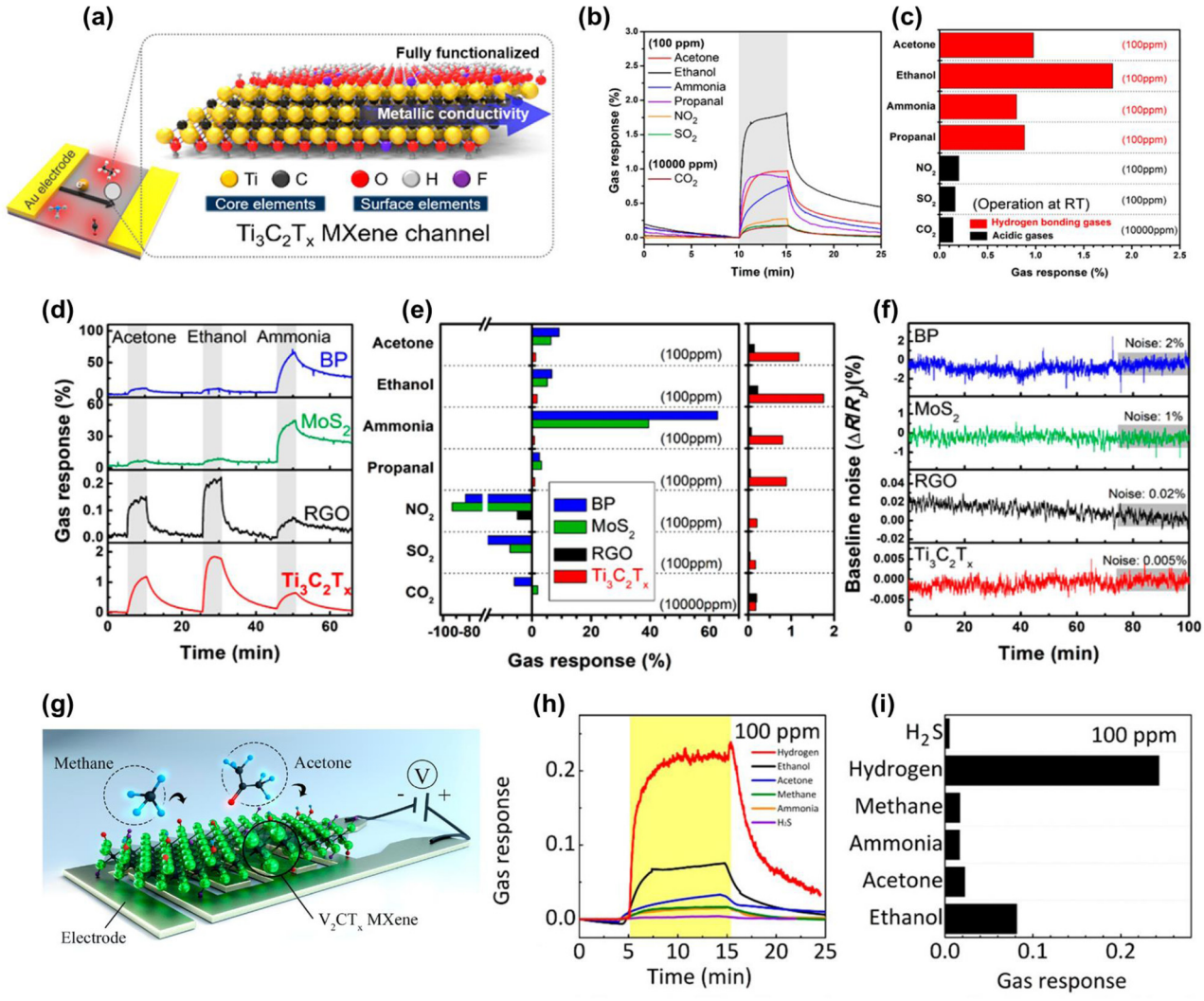

Fig. 4. Gas sensors based on pristine MXenes. (a) Schematic illustration of $Ti_3C_2T_x$ gas sensors with their structural and surface characterizations. (b) Dynamic response and (c) response plots of $Ti_3C_2T_x$ sensors to 100 ppm of acetone, ethanol, ammonia, propanal, NO_2, SO_2, and 10000 ppm of CO_2 at room temperature. (d) Gas response behaviors and (e) response plots of BP, MoS_2, RGO, and $Ti_3C_2T_x$ sensors to 100 ppm of various gases. (f) Electrical noise levels of the sensors under N_2 exposure. Reprinted with permission from Ref. [21], Copyright (2018) American Chemical Society. (g) Schematic illustration of a V_2CT_x gas sensor. (h) Dynamic gas response and (i) response plots of V_2CT_x gas sensor to 100 ppm of H_2, ethanol, acetone, methane, ammonia, and H_2S at room temperature. Reprinted with permission from Ref. [48], Copyright (2019) American Chemical Society.

highlight the effectiveness of pristine MXenes for rapid, sensitive, and low-noise gas detection.

3.2 Gas Sensors Based on Surface Functionalized MXenes

Various studies have focused on controlling the surface chemistry of MXenes to enhance their sensitivity and selectivity to target gases. MXene surfaces contain diverse functional groups (–O,–OH, and–F) that influence gas adsorption properties. Density functional theory (DFT) calculations indicated that the-OH-terminated MXene strongly adsorbed acidic molecules, whereas the-F-terminated group improved the hydrophobicity and enhanced the humidity stability for practical sensor applications. Chen et al. demonstrated surface-functionalized $Ti_3C_2T_x$ MXenes with superhydrophobic fluoroalkylsilane protective layers, specifically (3-chloropropyl) trimethoxysilane (CPTMS) and 1*H*,1*H*,2*H*,2*H*-perfluorooctyltriethoxysilane (FOTS), termed $Ti_3C_2T_x$-Cl and $Ti_3C_2T_x$-F, respectively [25]. $Ti_3C_2T_x$ nanosheets were synthesized from Ti_3AlC_2 via LiF/HCl etching (Fig. 5 (a)). After surface functionalization with CPTMS and FOTS, Brunauer-Emmett-Teller (BET) analysis showed increased surface areas of 20.4 m^2/g for $Ti_3C_2T_x$-Cl and 32.9 m^2/g for $Ti_3C_2T_x$-F. Water contact

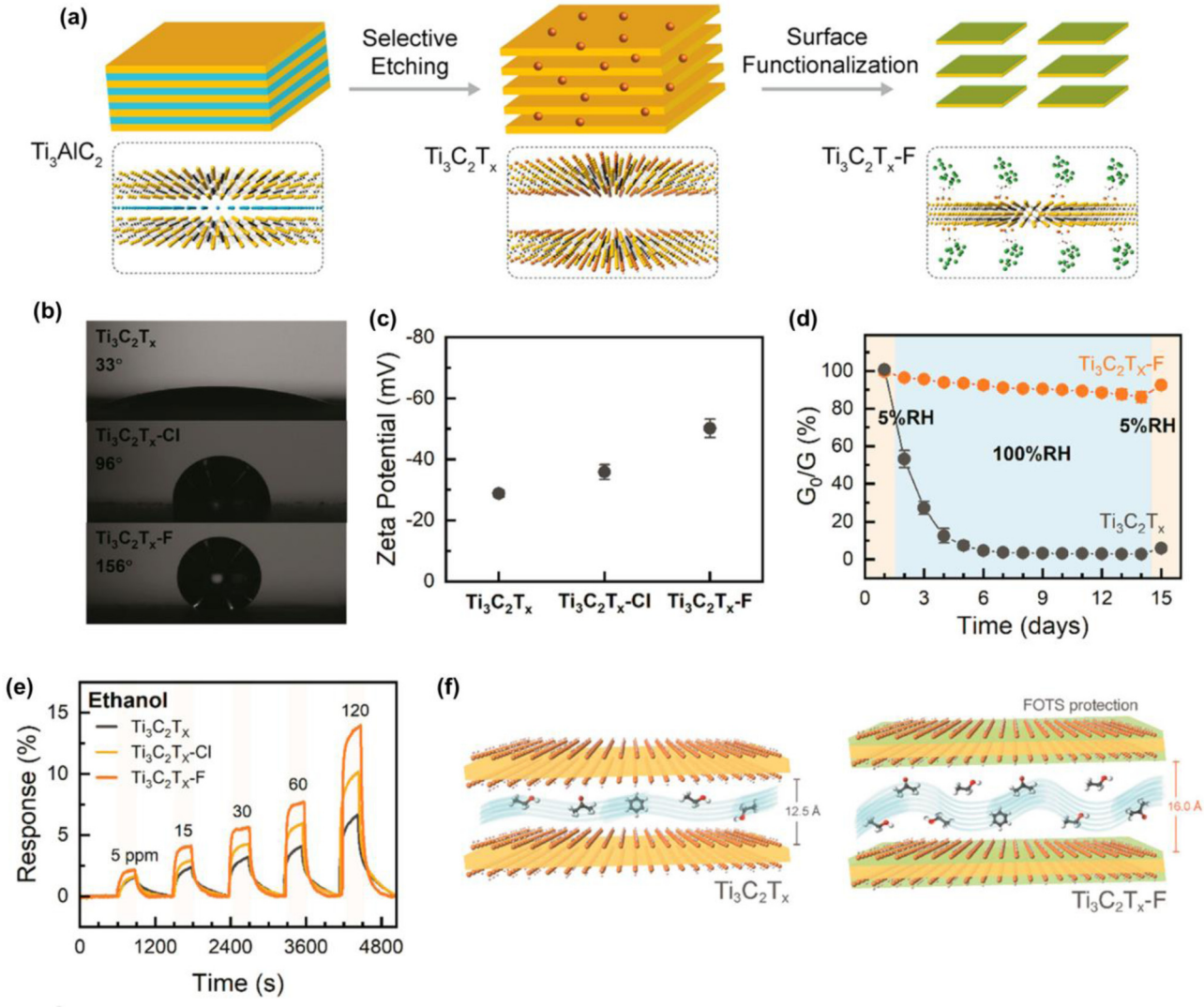

Fig. 5. Gas sensors based on surface functionalized MXenes. (a) Schematic illustration of $Ti_3C_2T_x$ functionalization for surface modification (b) Water contact angle measurements of $Ti_3C_2T_x$, $Ti_3C_2T_x$-Cl, and $Ti_3C_2T_x$-F film. (c) Zeta potential of $Ti_3C_2T_x$, $Ti_3C_2T_x$-Cl, and $Ti_3C_2T_x$-F film. (d) Changes in electrical conductance of $Ti_3C_2T_x$ and $Ti_3C_2T_x$-F under 5% and 100% RH over two weeks. (e) Comparison of gas responses for the MXene sensors. (f) Schematic illustration of $Ti_3C_2T_x$ and $Ti_3C_2T_x$-F under VOCs exposure. Reprinted with permission from Ref. [25], Copyright (2020) American Chemical Society.

angle measurements demonstrated enhanced hydrophobicity, with values of 96° for $Ti_3C_2T_x$-Cl and 156° for $Ti_3C_2T_x$-F, compared to 33° °for pristine MXene (Fig. 5 (b)). Zeta-potential measurements also confirmed increased surface charge, with $Ti_3C_2T_x$-Cl and $Ti_3C_2T_x$-F exhibiting more negative zeta potentials of -35.8 mV and -50.1 mV, respectively, compared to -28.7 mV for pristine $Ti_3C_2T_x$ (Fig. 5 (c)). These results indicate a substantial increase in the hydrophobicity of the FOTS and CPTMS functionalizations. To assess environmental stability, pristine $Ti_3C_2T_x$ and $Ti_3C_2T_x$-F were stored under 5% and 100% relative humidity (RH) conditions (Fig. 5 (d)). Both the materials exhibited stable electrical conductance under dry conditions (5% RH). However, at 100% RH, pristine MXene rapidly degraded to only 2.7% of its initial conductance, whereas $Ti_3C_2T_x$-F retained 92.5%, indicating effective humidity protection. Sensor performance evaluation with ethanol concentration ranging from 5 ppm to 120 ppm at room temperature showed consistently higher responses ($\Delta R/R_b$ (%)) for $Ti_3C_2T_x$-F compared to pristine $Ti_3C_2T_x$ (Fig. 5 (e)). In addition, $Ti_3C_2T_x$-F exhibits a nearly linear response ($R^2 > 0.98$). DFT calculations supported these experimental results, revealing a higher ethanol adsorption energy for $Ti_3C_2T_x$-F (-0.745 eV) compared to pristine $Ti_3C_2T_x$ (-0.621 eV). Moreover, the interlayer distance of $Ti_3C_2T_x$ increased from 12.5 to 16.0 Å after FOTS functionalization, which facilitated gas diffusion, leading to enhanced gas detection (Fig. 5 (f)). Thus, surface

functionalization with FOTS protection improved both humidity stability and ethanol detection capabilities.

Kim et al. demonstrated surface-functionalized MXenes using ADOPA ligands for enhanced sensitivity to NH_3 and VOCs along with improved long-term stability [24]. $Ti_3C_2T_x$ MXene sheets were synthesized from the Ti_3AlC_2 MAX phase using a LiF/HCl etching solution. Amphiphilic ADOPA ligands, produced by the esterification of DOPA and perfluoroalcohol derivatives, were grafted onto the MXene surfaces. The catechol groups within the ADOPA ligands form strong hydrogen bonds with the-OH groups on the MXene surface. Moreover, the fluorocarbon tail groups impart hydrophobicity to the MXene films. Ultrathin ADOPA-functionalized MXene films (AD1MX) approximately 10 nm thick were fabricated using a solvent-solvent interfacial self-assembly method, resulting in uniform and well-stacked MXene layers. Surface energy measurements showed increased hydrophobicity, with water contact angles of 95° for AD1MX compared to 63° for pristine $Ti_3C_2T_x$, reflecting the contribution of the fluorocarbon groups. Gas-sensing performance tests were conducted at room temperature on MXene films prepared by self-assembly and spin coating for acetone, ethanol, ammonia, and NO_2 detection at a concentration of 100 ppm. The films fabricated by self-assembly exhibited a higher response than the spin-coated samples across all the gases tested. Further comparison of self-assembled MXene films fabricated using ethanol/toluene (AD1MX_E/T) and acetone/toluene (AD1MX_A/T) solvents AD1MX_E/T exhibited a higher response than AD1MX_A/T for all gas types. Compared to pristine $Ti_3C_2T_x$, AD1MX_E/T exhibited notably enhanced responses, which were attributed to ADOPA ligand functionalization. DFT calculations confirmed stronger NH_3 adsorption on AD1MX (-0.59 eV) compared to pristine $Ti_3C_2T_x$ (-0.49 eV). Similar results were observed when applying ADOPA to other MXene materials such as $Mo_2TiC_2T_x$, demonstrating its broad applicability in enhancing gas sensor performance. These findings highlight the effectiveness of surface functionalization strategies in improving both the humidity stability and sensitivity to target gas molecules in MXene-based sensors.

3.3 Gas Sensors Based on MXene/Nanomaterial Heterostructures

MXene-based gas sensors incorporate nanocomposite heterostructures to enhance the gas detection performance. Combining MXenes with nanomaterials such as metal oxides (ZnO [51], SnO_2 [27], and WO_3 [52]), TMDs (SnS_2 [53], WS_2 [54], WSe_2 [55]), graphene [56], and metal-organic frameworks (MOFs) [57] exploits the advantages of each material to increase active sites For example, heterostructures involving metal oxides or TMDs can induce surface band bending, expanding the Debye region and thus improving both sensitivity and selectivity [58].

Chen et al. developed a heterostructure sensor composed of $Ti_3C_2T_x$ MXene nanosheets and WSe_2 nanoflakes prepared via liquid-phase exfoliation to achieve selective ethanol detection. $Ti_3C_2T_x$ was synthesized by HF etching, and the WSe_2 nanoflakes were exfoliated in cetyltrimethylammonium bromide (CTAB) to form positively charged CTA^+-WSe_2 flakes (Fig. 6 (a)). Mixing the negatively charged $Ti_3C_2T_x$ (zeta potential: -29.5 mV, due to -OH and -O functional groups) with the positively charged CTA^+-WSe_2 (zeta potential: +30 mV) led to electrostatic attraction and stable heterojunction formation. Gas-sensing tests under ethanol exposure (1–40 ppm) at room temperature revealed distinct sensing behaviors, characterized by increased resistance to gas exposure and incomplete recovery owing to the adsorption of ethanol molecules. Conversely, the $Ti_3C_2T_x/WSe_2$ heterostructure exhibited n-type sensing behavior with decreasing resistance upon ethanol exposure and improved recovery. The response slope (response per ppm) for $Ti_3C_2T_x/WSe_2$ was approximately 12-fold greater than that for pristine $Ti_3C_2T_x$ without saturation, even at higher ethanol concentrations. The improved sensing performance was attributed to the efficient electron transport facilitated by the $Ti_3C_2T_x/WSe_2$ heterojunction. $Ti_3C_2T_x$ nanosheets with high conductivity supplied electrons to WSe_2, forming junctions that enhanced the catalytic activity and reduced the number of carrier-depletion layers. Upon ethanol exposure, adsorbed oxygen reacts with ethanol molecules, releasing electrons into the conduction band, thereby reducing the depletion region and improving the sensor response. Additionally, $Ti_3C_2T_x/WSe_2$ demonstrated enhanced humidity stability (Fig. 6 (c)). After exposure to 80% RH for over 10 days, $Ti_3C_2T_x/WSe_2$ maintained 88% of its initial resistance and recovered to 92% in a dry environment, whereas pristine $Ti_3C_2T_x$ degraded to only 21% of its original resistance. The flexible $Ti_3C_2T_x/WSe_2$ sensors, fabricated via inkjet printing, maintained a consistent response to ethanol after 1000 bending cycles (radius = 5 mm), demonstrating stable mechanical flexibility and sustained electrical performance under mechanical deformation (Figs. 6 (d) and (e)).

Kim et al. demonstrated a MoS_2/MXene heterostructured aerogel-based gas sensor designed for NO_2 detection [59]. $Ti_3C_2T_x$ MXene sheets were synthesized by selectively etching an Al layer from Ti_3AlC_2 using a LiF/HCl solution. MoS_2 nanosheets were prepared from bulk MoS_2 powder using hydrazine-assisted ball milling. The prepared $Ti_3C_2T_x$ and MoS_2 nanosheets were assembled into MoS_2/MXene gels by mixing in an aqueous solution, facilitated by the similar hydrophilicity and negatively charged surfaces of the two materials. During freeze casting, the $Ti_3C_2T_x$ sheets were

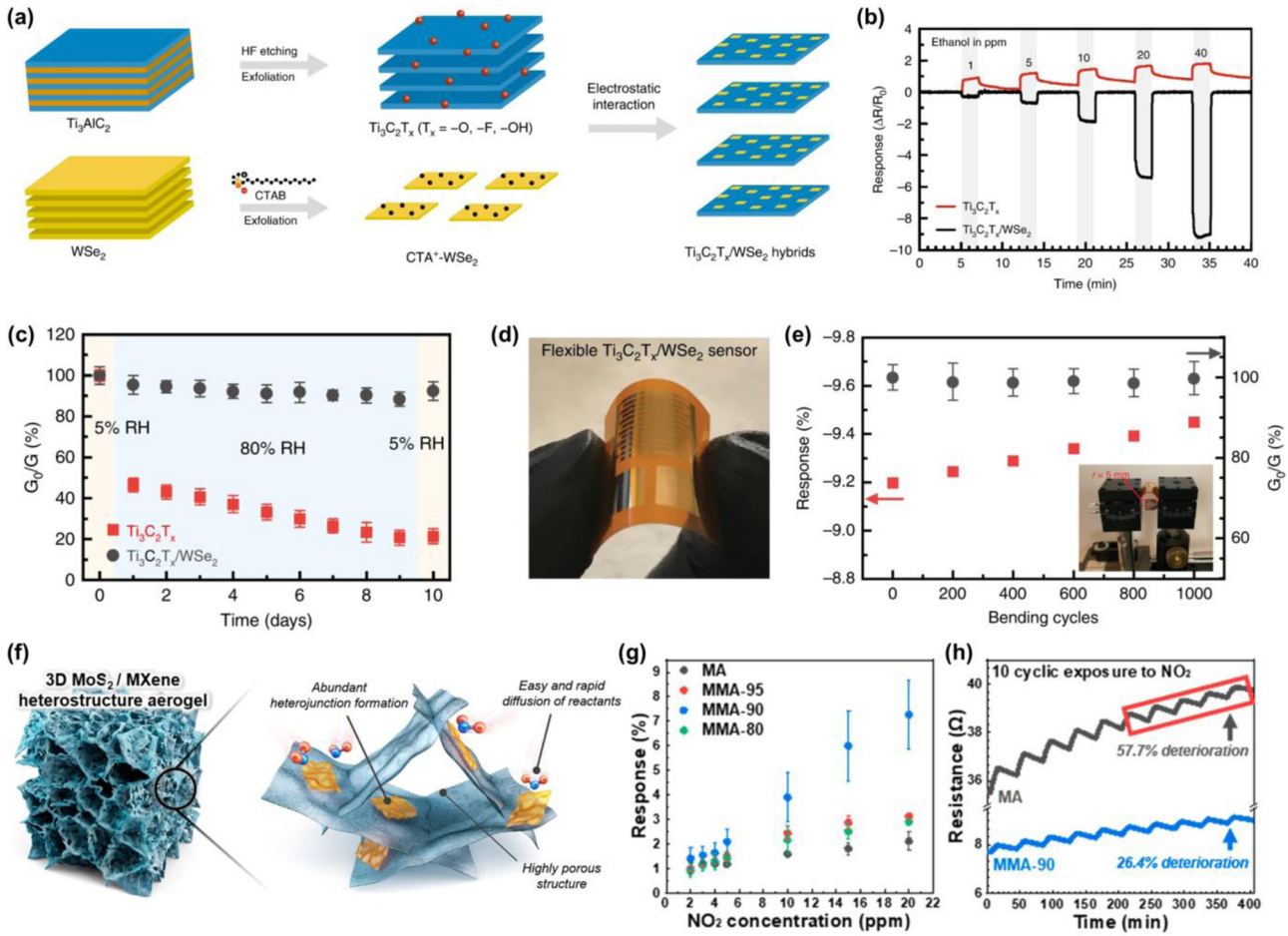

Fig. 6. Gas sensors based on MXene/nanomaterials heterostructures. (a) Schematic illustration of the synthesis process of $Ti_3C_2T_x$/WSe_2 nanohybrids. (b) Dynamic response of $Ti_3C_2T_x$ and $Ti_3C_2T_x$/WSe_2 sensors to 1-400 ppm of C_2H_5OH. (c) Variation in electrical conductance of $Ti_3C_2T_x$ and $Ti_3C_2T_x$/WSe_2 sensors under 5% and 80% RH over 10 days. (d) Optical image of a flexible $Ti_3C_2T_x$/WSe_2 sensor. (e) Changes in C_2H_5OH sensing response and electrical conductance under bending cycles. Reprinted with permission from Ref. [28], Copyright (2020) Springer Nature. (f) Schematic illustration of the 3D MoS_2/MXene heterostructure aerogel. (g) Gas-sensing responses toward 2-20 ppm of NO_2 for pristine MXene aerogel (MA) and MoS_2/MXene heterostructure aerogels (MMA). (h) 10 cycle exposures and recoveries to 10 ppm of NO_2 on MA and MMA-90. Reprinted with permission from Ref. [59], Copyright (2023) American Chemical Society.

interconnected to form a continuous three-dimensional (3D) network, with MoS_2 nanosheets assembled uniformly onto the MXene frameworks. After freeze-drying, a MoS_2/MXene composite aerogel (MMA) was obtained and designated as MMA-*X*, where *X* represents the mass percentage of $Ti_3C_2T_x$ in the aerogel. The hierarchical 3D aerogel structure exhibited abundant heterojunctions and a highly porous framework, enabling efficient transport of analyte gases throughout the network (Fig. 6 (f)). The MMA demonstrated ultralow apparent density and an ultralight structure, capable of standing freely on a dandelion seed. These lightweight and porous characteristics are advantageous for applications requiring portability and space constraints, including wearable gas sensors. The gas-sensing performance of the MA (pure MXene aerogel) and MMA-*X* samples (MMA-95, MMA-90, and MMA-80) was evaluated with NO_2 concentrations ranging from 1 to 20 ppm (Fig. 6 (g)). Increasing the MoS_2 content in the MMA-*X* samples enhanced the sensors' response to NO2, demonstrating the catalytic effect of MoS_2 decoration on the aerogel structure. Notably, the MMA-90 sample exhibited a response of 3.91% ($\Delta R/R_b$ (%)) upon exposure to 10 ppm of NO_2, approximately 2.5 times higher than the response of MA. Cyclic tests involving 10 repeated exposure and recovery cycles at 10 ppm NO_2 were conducted using MA and MMA-90 (Fig. 6 (h)). After five cycles, the response of MA degraded to 57.7% of the initial cycle's response, while MMA-90 retained higher stability, retaining 26.4% of its initial response. These results highlight the potential of MXene-based heterostructured aerogels as robust and sensitive architectures for chemoresistive gas-sensing applications.

4. PERSPECTIVES AND CHALLENGES

MXenes have attracted significant attention as sensing materials for room-temperature chemoresistive gas sensors, particularly for the detection of NO_2, NH_3, and VOCs. The key properties of MXenes, including their high electrical conductivity, abundant surface functional groups, mechanical flexibility, and high surface-to-volume ratio, provide distinct advantages for gas detection. High electrical conductivity enables rapid electron transport upon gas adsorption, facilitating fast response and recovery. In addition, the intrinsically low signal-to-noise ratio allows for the detection of gases at low concentrations. MXene surfaces possess diverse functional groups, such as -O, -OH, and -F, which directly interact with the target gases. Specific functional groups selectively enhance the sensor responses to certain gases. For instance, -O groups strongly interact with NO_2, -OH groups facilitate the binding of acidic gases through hydrogen bonding, and -F groups enhance the sensor stability under humid conditions. MXenes such as $Ti_3C_2T_x$, $V_3C_2T_x$, and $Mo_3C_2T_x$ are effective active layers in chemoresistive gas sensing.

Despite these promising properties, MXene-based sensors currently face several critical limitations, including instability in ambient air and moisture, insufficient sensor response compared to conventional metal oxide sensors, and limited gas selectivity. Regarding instability, MXenes are prone to oxidation in air and humidity, forming oxidized species (e.g., TiO_2 in $Ti_3C_2T_x$). To address oxidation, protective layers such as PDMS and polyimide, and polymeric functional coatings such as FOTS and ADOPA have been effectively employed. The low response signal of MXene sensors compared to conventional metal-oxide-based gas sensors complicates practical electronic integration and signal detection. Constructing heterostructures between MXene and various nanomaterials (e.g., metal oxides, TMD, graphene, and MOF) enhances the sensing response through junction effects and improves catalytic activity. However, the limited gas selectivity, due to MXenes' broad reactivity with various gases, remains a challenge. Functionalization strategies involving noble metal nanoparticles (Au, Pd, Pt, and Ag) enhance selective responses through chemical and electronic sensitization mechanisms [60,61].

Future directions for MXene-based gas sensors include the development of sensor arrays [62], IoT applications [63], photoactivated sensors [64], and neuromorphy-integrated sensors [65]. Sensor arrays based on MXene heterostructures or noble metal decorations enable the discrimination of complex gas mixtures using principal component analysis (PCA) and machine learning methods [66]. Photoactivated MXene gas sensors utilize high-optical-absorption materials to further enhance sensor responses and reduce response and recovery times at room temperature [67]. The flexibility and room-temperature operability of MXene-based sensors support their application in biocompatible gas sensing, expanding the scope of IoT implementations for wearable devices. Finally, integrating MXene sensors with neuromorphic architectures that mimic biological olfactory functions, such as stimulus-dependent synaptic plasticity, short- and long-term memory, and analog signal modulation, can enable multimodal sensing, low-power operations, and effective interfaces with artificial intelligence technologies [68].

5. CONCLUSION

This review comprehensively discusses the MXene synthesis methods, fundamental sensing mechanisms, and recent advances in gas sensors that employ MXenes. Strategies to address current limitations of MXenes, such as humidity sensitivity, low selectivity, and limited sensor responses, have been highlighted, with a focus on surface functionalization and heterostructure formation approaches. To overcome these challenges, MXene-based sensors show promise as alternatives to conventional gas sensors, especially for wearable and biocompatible applications that require reliable room-temperature operation. Continued research efforts aimed at optimizing MXene properties, stabilizing performance under environmental conditions, and integrating MXenes with advanced technologies will enable MXene-based chemoresistive gas sensors to effectively meet future sensing demands.

CRediT Authorship Contribution Statement

Gi Baek Nam: Investigation, Data curation, Methodology, Visualization, Writing—original draft, writing —review, and editing. **Ho Won Jang:** Conceptualization, Project administration, Supervision, Writing, review, and editing.

Declaration of Competing Interest

The authors declare that they have no competing financial interests or personal relationships that may have influenced the work reported in this study.

Acknowledgements

This research was supported by the Nano & Material Technology Development Program through the National Research Foundation of Korea (NRF), funded by the Ministry of Science and ICT(RS-2024-00405016). This work was financially supported by the Cooperative Research Program for Agriculture Science and Technology Development (Project No. PJ01706703) of the Rural Development Administration, Republic of Korea. The Inter-University Semiconductor Research Center and Institute of Engineering Research at Seoul National University provided research facilities for this study.

REFERENCES

[1] S.C. Mukhopadhyay, S.K.S. Tyagi, N.K. Suryadevara, V. Piuri, F. Scotti, S. Zeadally, Artificial intelligence-based sensors for next generation IoT applications: A review, IEEE Sens. J. 21 (2021) 24920–24932.

[2] F. Zhou, Y. Chai, Near-sensor and in-sensor computing, Nat. Electron. 3 (2020) 664–671.

[3] S. Lee, S. Kim, G.B. Nam, T.H. Eom, H.W. Jang, Chemoresistive Gas Sensors for Food Quality Monitoring, J. Semicond. Technol. Sci. 22 (2022) 244–258.

[4] X. Zhou, Z. Xue, X. Chen, C. Huang, W. Bai, Z. Lu, et al., Nanomaterial-based gas sensors used for breath diagnosis, J. Mater. Chem. B 8 (2020) 3231–3248.

[5] S.H. Cho, J.M. Suh, B. Jeong, T.H. Lee, K.S. Choi, T.H. Eom, et al., Substantially accelerated response and recovery in Pd-decorated WO_3 nanorods gasochromic hydrogen sensor, Small 20 (2024) 2309744.

[6] S.Y. Jeong, J.S. Kim, J.H. Lee, Rational design of semiconductor-based chemiresistors and their libraries for next-generation artificial olfaction, Adv. Mater. 32 (2020) 2002075.

[7] D.Y. Nadargi, A. Umar, J.D. Nadargi, S.A. Lokare, S. Akbar, I.S. Mulla, et al., Gas sensors and factors influencing sensing mechanism with a special focus on MOS sensors, J. Mater. Sci. 58 (2023) 559–582.

[8] S.J. Park, S.M. Lee, J. Lee, S. Choi, G.B. Nam, Y.K. Jo, et al., Pd-$W_{18}O_{49}$ Nanowire MEMS Gas Sensor for Ultraselective Dual Detection of Hydrogen and Ammonia, Small 21 (2025) 2405809.

[9] G.B. Nam, T.H. Eom, S.H. Cho, Y.J. Kim, S. Choi, W.S. Cheon, et al., Maximized nanojunctions in Pd/SnO_2 nanoparticles for ultrasensitive and rapid H_2 detection, Chem. Eng. J. 494 (2024) 153116.

[10] N. Barsan, U. Weimar, Conduction model of metal oxide gas sensors, J. Electroceram. 7 (2001) 143–167.

[11] Y. Kim, T. Kim, J. Lee, Y.S. Choi, J. Moon, S.Y. Park, et al., Tailored Graphene Micropatterns by Wafer-Scale Direct Transfer for Flexible Chemical Sensor Platform, Adv. Mater. 33 (2021) 2004827.

[12] W. Yuan, G. Shi, Graphene-based gas sensors, J. Mater. Chem. A 1 (2013) 10078–10091.

[13] S.J. Kim, G.B. Nam, Y.J. Kim, T.H. Eom, J.-E. Ryu, H.J. Kim, et al., Ambient Stable $CsCu_2I_3$ Flexible Gas Sensors for Reliable NO_2 Detection at Room Temperature, Nano Lett. (2025) 2894–2902.

[14] T. Pham, G. Li, E. Bekyarova, M.E. Itkis, A. Mulchandani, MoS_2-based optoelectronic gas sensor with sub-parts-per-billion limit of NO_2 gas detection, ACS Nano 13 (2019) 3196–3205.

[15] D. Liu, Z. Tang, Z. Zhang, Comparative study on NO_2 and H_2S sensing mechanisms of gas sensors based on WS_2 nanosheets, Sens. Actuators B Chem. 303 (2020) 127114.

[16] S.M. Lee, Y.J. Kim, S.J. Park, W.S. Cheon, J. Kim, G.B. Nam, et al., In-Situ Growth of 2D MOFs as a Molecular Sieving Layer on SnS_2 Nanoflakes for Realizing Ultraselective H_2S Detection, Adv. Funct. Mater. 35 (2025) 2417019.

[17] A. VahidMohammadi, J. Rosen, Y. Gogotsi, The world of two-dimensional carbides and nitrides (MXenes), Science 372 (2021) eabf1581.

[18] H.J. Kim, C.W. Lee, S. Park, S. Choi, S.H. Park, G.B. Nam, et al., MXene-based high performance microfluidic pH sensors for electronic tongue, Sens. Actuators B Chem. 409 (2024) 135636.

[19] Z. Guo, L. Gao, Z. Xu, S. Teo, C. Zhang, Y. Kamata, et al., High electrical conductivity 2D MXene serves as additive of perovskite for efficient solar cells, Small 14 (2018) 1802738.

[20] Y. Wang, J. Fu, J. Xu, H. Hu, D. Ho, Atomic plasma grafting: precise control of functional groups on $Ti_3C_2T_x$ MXene for room temperature gas sensors, ACS Appl. Mater. Interfaces 15 (2023) 12232–12239.

[21] S.J. Kim, H.-J. Koh, C.E. Ren, O. Kwon, K. Maleski, S.-Y. Cho, et al., Metallic $Ti_3C_2T_x$ MXene gas sensors with ultrahigh signal-to-noise ratio, ACS Nano 12 (2018) 986–993.

[22] W.-N. Zhao, N. Yun, Z.-H. Dai, Y.-F. Li, A high-performance trace level acetone sensor using an indispensable $V_4C_3T_x$ Mxene, RSC Adv. 10 (2020) 1261–1270.

[23] T. Thomas, J.A.R. Ramon, V. Agarwal, A. Álvarez-Méndez, J.A. Martinez, Y. Kumar, et al., Highly stable, fast responsive Mo_2CT_x MXene sensors for room temperature carbon dioxide detection, Microporous Mesoporous Mater. 336 (2022) 111872.

[24] S. Kim, T. Y. Ko, A. K. Jena, A. S. Nissimagoudar, J. Lee, S. Lee, et al., Instant Self-Assembly of Functionalized MXenes in Organic Solvents: General Fabrication to High-Performance Chemical Gas Sensors, Adv. Funct. Mater. 34 (2024) 2310641.

[25] W.Y. Chen, S.-N. Lai, C.-C. Yen, X. Jiang, D. Peroulis, L.A. Stanciu, Surface functionalization of $Ti_3C_2T_x$ MXene with highly reliable superhydrophobic protection for volatile organic compounds sensing, ACS nano 14 (2020) 11490–11501.

[26] A. Hermawan, B. Zhang, A. Taufik, Y. Asakura, T. Hasegawa, J. Zhu, et al., CuO nanoparticles/$Ti_3C_2T_x$ MXene hybrid nanocomposites for detection of toluene gas, ACS Appl. Nano Mater. 3 (2020) 4755–4766.

[27] T. He, W. Liu, T. Lv, M. Ma, Z. Liu, A. Vasiliev, et al., MXene/SnO_2 heterojunction based chemical gas sensors, Sens. Actuators B Chem. 329 (2021) 129275.

[28] W.Y. Chen, X. Jiang, S.-N. Lai, D. Peroulis, L. Stanciu, Nanohybrids of a MXene and transition metal dichalcogenide for selective detection of volatile organic compounds, Nat. Commun. 11 (2020) 1302.

[29] S. Hong, J.K. El-Demellawi, Y. Lei, Z. Liu, F.A. Marzooqi, H.A. Arafat, et al., Porous $Ti_3C_2T_x$ MXene membranes for highly efficient salinity gradient energy harvesting, ACS nano 16 (2022) 792–800.

[30] J. Chen, K. Chen, D. Tong, Y. Huang, J. Zhang, J. Xue, et al., CO_2 and temperature dual responsive "Smart" MXene phases, Chem. Commun. 51 (2015) 314–317.

[31] M. Naguib, O. Mashtalir, J. Carle, V. Presser, J. Lu, L. Hultman, et al., Two-dimensional transition metal carbides, ACS Nano 6 (2012) 1322–1331.

[32] J. Peng, X. Chen, W.-J. Ong, X. Zhao, N. Li, Surface and

heterointerface engineering of 2D MXenes and their nanocomposites: insights into electro-and photocatalysis, Chem 5 (2019) 18–50.
[33] T. Zhang, L. Pan, H. Tang, F. Du, Y. Guo, T. Qiu, et al., Synthesis of two-dimensional $Ti_3C_2T_x$ MXene using HCl+ LiF etchant: enhanced exfoliation and delamination, J. Alloys Compd. 695 (2017) 818–826.
[34] N. Goossens, K. Lambrinou, B. Tunca, V. Kotasthane, M.C. Rodríguez González, A. Bazylevska, et al., Upscaled Synthesis Protocol for Phase-Pure, Colloidally Stable MXenes with Long Shelf Lives, Small Methods 8 (2024) 2300776.
[35] M. Ghidiu, M.R. Lukatskaya, M.-Q. Zhao, Y. Gogotsi, M.W. Barsoum, Conductive two-dimensional titanium carbide 'clay'with high volumetric capacitance, Nature 516 (2014) 78–81.
[36] A. Qian, J.Y. Seo, H. Shi, J.Y. Lee, C.H. Chung, Surface functional groups and electrochemical behavior in dimethyl sulfoxide-delaminated $Ti_3C_2T_x$ Mxene, ChemSusChem 11 (2018) 3719–3723.
[37] S. Ren, J.-L. Xu, L. Cheng, X. Gao, S.-D. Wang, Amine-Assisted Delaminated 2D $Ti_3C_2T_x$ MXenes for High Specific Capacitance in Neutral Aqueous Electrolytes, ACS Appl. Mater. Interfaces 13 (2021) 35878–35888.
[38] O. Mashtalir, M. Naguib, V.N. Mochalin, Y. Dall'Agnese, M. Heon, M.W. Barsoum, et al., Intercalation and delamination of layered carbides and carbonitrides, Nat. Commun. 4 (2013) 1716.
[39] J. Xuan, Z. Wang, Y. Chen, D. Liang, L. Cheng, X. Yang, et al., Organic-base-driven intercalation and delamination for the production of functionalized titanium carbide nanosheets with superior photothermal therapeutic performance, Angew. Chem. 128 (2016) 14789–14794.
[40] C. Rong, T. Su, Z. Li, T. Chu, M. Zhu, Y. Yan, et al., Elastic properties and tensile strength of 2D $Ti_3C_2T_x$ MXene monolayers, Nat. Commun. 15 (2024) 1566.
[41] L. Jia, S. Zhou, A. Ahmed, Z. Yang, S. Liu, H. Wang, et al., Tuning MXene electrical conductivity towards multifunctionality, Chem. Eng. J. 475 (2023) 146361.
[42] R.A.B. John, K. Vijayan, N.L.W. Septiani, A. Hardiansyah, A.R. Kumar, B. Yuliarto, et al., Gas-sensing mechanisms and performances of MXenes and MXene-based heterostructures, Sensors 23 (2023) 8674.
[43] Y. Zhang, Y. Jiang, Z. Duan, Q. Huang, Y. Wu, B. Liu, et al., Highly sensitive and selective NO_2 sensor of alkalized V_2CT_x MXene driven by interlayer swelling, Sens. Actuators B Chem. 344 (2021) 130150.
[44] X. Li, Z. An, Y. Lu, J. Shan, H. Xing, G. Liu, et al., Room temperature VOCs sensing with termination-modified $Ti_3C_2T_x$ MXene for wearable exhaled breath monitoring, Adv. Mater. Technol. 7 (2022) 2100872.
[45] K. Rathi, N.K. Arkoti, K. Pal, Fabrication of delaminated 2D metal carbide MXenes (Nb_2CT_x) by CTAB-based NO_2 Gas Sensor with Enhanced Stability, Adv. Mater. Interfaces 9 (2022) 2200415.
[46] S.M. Majhi, A. Ali, Y.E. Greish, H.F. El-Maghraby, S.T. Mahmoud, V_2CT_X MXene-based hybrid sensor with high selectivity and ppb-level detection for acetone at room temperature, Sci. Rep. 13 (2023) 3114.
[47] Q. Zhao, W. Zhou, M. Zhang, Y. Wang, Z. Duan, C. Tan, et al., Edge-enriched $Mo_2TiC_2T_x/MoS_2$ heterostructure with coupling interface for selective NO_2 monitoring, Adv. Funct. Mater. 32 (2022) 2203528.
[48] E. Lee, A. VahidMohammadi, Y.S. Yoon, M. Beidaghi, D.-J. Kim, Two-dimensional vanadium carbide MXene for gas sensors with ultrahigh sensitivity toward nonpolar gases, ACS Sens. 4 (2019) 1603–1611.
[49] Y.-T. Wang, W.-T. Whang, C.-H. Chen, Hollow V_2O_5 nanoassemblies for high-performance room-temperature hydrogen sensors, ACS Appl. Mater. Interfaces 7 (2015) 8480–8487.
[50] X. Xu, M. Yin, N. Li, W. Wang, B. Sun, M. Liu, et al., Vanadium-doped tin oxide porous nanofibers: Enhanced responsivity for hydrogen detection, Talanta 167 (2017) 638–644.
[51] Z. Yang, L. Jiang, J. Wang, F. Liu, J. He, A. Liu, et al., Flexible resistive NO_2 gas sensor of three-dimensional crumpled MXene $Ti_3C_2T_x$/ZnO spheres for room temperature application, Sens. Actuators B Chem. 326 (2021) 128828.
[52] P. Wang, S. Guo, Y. Zhao, Z. Hu, Y. Tang, L. Zhou, et al., WO_3 nanoparticles supported by Nb_2CT_x MXene for superior acetone detection under high humidity, Sens. Actuators B Chem. 398 (2024) 134710.
[53] T. He, S. Sun, B. Huang, X. Li, MXene/SnS_2 heterojunction for detecting sub-ppm NH_3 at room temperature, ACS Appl. Mater. Interfaces 15 (2023) 4194–4207.
[54] S. Sardana, A. Debnath, D. Aswal, A. Mahajan, WS_2 nanosheets decorated multi-layered MXene based chemiresistive sensor for efficient detection and discrimination of NH_3 and NO_2, Sens. Actuators B Chem. 394 (2023) 134352.
[55] B. Maji, S. Badhulika, Fully Flexible WSe_2/V_2C MXene Heterostructure-based Gas Sensor: a detailed Sensing Analysis for ppb level Detection of Ammonia at Room Temperature, J. Alloys Compd. 1017 (2025) 179079.
[56] S.H. Lee, W. Eom, H. Shin, R.B. Ambade, J.H. Bang, H.W. Kim, et al., Room-temperature, highly durable $Ti_3C_2T_x$ MXene/graphene hybrid fibers for NH_3 gas sensing, ACS Appl. Mater. Interfaces 12 (2020) 10434–10442.
[57] N.K. Arkoti, K. Pal, $Ti_3C_2T_x$ MXene-Derived Metal–Organic Frameworks for Room Temperature NO_2 Detection, ACS Appl. Mater. Interfaces 17 (2025) 31316–31325.
[58] M. Mathew, P.V. Shinde, R. Samal, C.S. Rout, A review on mechanisms and recent developments in pn heterojunctions of 2D materials for gas sensing applications, J. Mater. Sci. 56 (2021) 9575–9604.
[59] S. Kim, H. Shin, J. Lee, C. Park, Y. Ahn, H.J. Cho, et al., Three-Dimensional MoS_2/MXene Heterostructure Aerogel for Chemical Gas Sensors with Superior Sensitivity and Stability, ACS Nano 17 (2023) 19387–19397.
[60] X. Li, L. Jin, A. Ni, L. Zhang, L. He, H. Gao, et al., Tough and antifreezing MXene@ Au hydrogel for low-temperature trimethylamine gas sensing, ACS Appl. Mater. Interfaces 14 (2022) 30182–30191.
[61] W.Y. Chen, C.D. Sullivan, S.-N. Lai, C.-C. Yen, X. Jiang, D. Peroulis, et al., Noble-Nanoparticle-Decorated Ti-C_2T_x MXenes for Highly Sensitive Volatile Organic Compound

Detection, ACS Omega 7 (2022) 29195–29203.
[62] D. Li, G. Liu, Q. Zhang, M. Qu, Y. Q. Fu, Q. Liu, et al., Virtual sensor array based on MXene for selective detections of VOCs, Sens. Actuators B Chem. 331 (2021) 129414.
[63] R. Yuan, Y. Yang, B. Zou, Y. Zhang, MXene-enabled gas sensors for wearable breath monitoring, Chem. Eng. J. 510 (2025) 161414.
[64] G.B. Nam, J.-E. Ryu, T.H. Eom, S.J. Kim, J.M. Suh, S. Lee, et al., Real-time tunable gas sensing platform based on SnO_2 nanoparticles activated by blue micro-light-emitting diodes, Nano Micro Lett. 16 (2024) 261.
[65] J.K. Han, M. Kang, J. Jeong, I. Cho, J.M. Yu, K.J. Yoon, et al., Artificial olfactory neuron for an in-sensor neuromorphic nose, Adv. Sci. 9 (2022) 2106017.
[66] S.-H. Sung, J.M. Suh, Y.J. Hwang, H.W. Jang, J.G. Park, S.C. Jun, Data-centric artificial olfactory system based on the eigengraph, Nat. Commun. 15 (2024) 1211.
[67] T. Zhou, P. Zhang, Z. Yu, M. Tao, D. Zhou, B. Yang, et al., Light-driven, ultra-sensitive and multifunctional ammonia wireless sensing system by plasmonic-functionalized Nb_2CT_x MXenes towards smart agriculture, Nano Energy 108 (2023) 108216.
[68] Y. Deng, M. Zhao, Y. Ma, S. Liu, M. Liu, B. Shen, et al., A Flexible and Biomimetic Olfactory Synapse with Gasotransmitter-Mediated Plasticity, Adv. Funct. Mater. 33 (2023) 2214139.

Gi Baek Nam is currently a PhD candidate under the supervision of Prof. Ho Won Jang of the Department of Materials Science and Engineering at Seoul National University (SNU). He received his BS degree in Materials Science and Engineering from Korea University in 2022. His research has focused on chemoresistive gas sensors based on metal oxides and sulfides for use in electronic noses.

Ho Won Jang is a professor in the Department of Materials Science and Engineering at Seoul National University. He earned his Ph.D. in Materials Science and Engineering from Pohang University of Science and Technology in 2004. From 2006 to 2009, he worked as a research associate at the University of Wisconsin, Madison. Before joining Seoul National University in 2012, he served as a senior research scientist at the Korea Institute of Science and Technology. His research interests include the synthesis of oxides, 2D materials, and halide perovskites, as well as their applications in chemical sensors, nanoelectronics, solar water-splitting cells, plasmonics, metal–insulator transitions, and ferroelectricity.